Bio-Derived Chitosan Additive Enables Anion anchoring and Zn(002) Deposition for High-Performance Zn anode

Guanglu Jiang,[a,b] Luoyuan Guo,[a,b] Mingbo Shao,[a,b] Najun Liu,[a,b] Zhongchao Bai,[c] Nana Wang,*[d] Huili Peng,*[a,b] Xiaolei Jiang*[a,b]

[a] School of Chemistry and Chemical Engineering, Linyi University, Linyi 276000, P. R. China. E-mail: penghuili@lyu.edu.cn, jiangxiaolei@lyu.edu.cn

[b] Key Laboratory of Advanced Biomaterials and Nanomedicine in Universities of Shandong, Linyi University, Linyi, 276000, P. R. China. E-mail: penghuili@lyu.edu.cn, jiangxiaolei@lyu.edu.cn

[c] Institute of Energy Materials Science, University of Shanghai for Science and Technology, Shanghai, 200093 P. R. China

[d] Centre for Clean Energy Technology, School of Mathematical and Physical Sciences, Faculty of Science, University of Technology Sydney, Sydney, 2007, NSW, Australia. E-mail: Nana.Wang@uts.edu.au.

Experimental Section

Material synthesis

Chitosan (CS, deacetylation degree ≥95%, MW 161.16, 0.5 g) was dispersed in 30 mL of deionized water. Subsequently, 150 μL of glacial acetic acid (99.5%) was added to the suspension to completely dissolve the CS. Glycidyl trimethylammonium chloride (GTMAC, purity ≥90%) was then introduced dropwise into CS solution. The reaction system was maintained in a water bath at 65 °C for 18 h to facilitate quaternization. Following the reaction, the crude product was precipitated by gradual addition of acetone. The resulting precipitate was collected via vacuum filtration, sequentially washed with acetone to remove unreacted reagents, and finally dried under vacuum at 60°C for 24 h to obtain the water-soluble chitosan quaternary ammonium derivative (HACC).

Preparation of electrolyte

2 M $ZnSO_4$ electrolyte solution (denoted as BE) was prepared by dissolving $ZnSO_4{\cdot}7H_2O$ (Sinopharm Group, purity ≥99.5%) in deionized water. Subsequently, the HACC-modified electrolyte (denoted as HACC-BE) was prepared by dissolved an appropriate amount of HACC and 2 M $ZnSO_4$ in deionized water. The concentration of HACC in the composite electrolyte was controlled by adjusting the mass of HACC during the preparation of the solution.

Preparation of LMO cathode electrode

The cathode electrode was fabricated using $LiMn_2O_4$ (LMO, Cyber) as the active material. A cathode slurry was prepared by homogenizing 90 wt% LMO, 3 wt% acetylene black (AB, DodoChem), 3 wt% multi-walled carbon nanotubes (MWCNTs, XF Nano), and 4 wt% polyvinylidene fluoride (PVdF, Solvay 5130 binder, DodoChem) in N-methyl-2-pyrrolidone (NMP, 99.5% purity, Aladdin). The slurry was uniformly blade-coated onto carbon paper and dried at 60°C for 8 h under vacuum. The active material mass loading was precisely controlled at ~16 mg cm^{-2} through

gravimetric calibration.

Electrochemical Measurements

The electrochemical properties were evaluated by assembling CR2025-type coin cells and pouch cells. Separator membranes (GF/F, Whatman) were employed for cell assembly. In asymmetric cells, Zn foil (99.99% purity, Cyber) and Cu foil (Cyber) served as negative and positive electrodes, respectively. Symmetric cells utilized identical Zn electrodes. BE or HACC-BE served as the electrolyte. Full cells were constructed using a 10 μm Zn anode paired with LMO cathodes, maintaining an N/P capacity ratio of ~3.2. The electrolytes consisted of either BE (2 M Li_2SO_4 + 1 M $ZnSO_4$) or HACC-BE (2 M Li_2SO_4 + 1 M $ZnSO_4$ + HACC).

Electrochemical measurements were conducted using a LAND Battery Cycler (CT 2001A, China). Linear sweep voltammetry (LSV) and linear polarization (LP) measurements were tested on an electrochemical workstation (CHI 760E, China). Electrochemical impedance spectroscopy (EIS) of cells measurements were performed on an electrochemical workstation (Metrohm Autolab 302N, Switzerland) in a frequency range 0.01-10^5 Hz.

The transfer number of Zn^{2+} (t_{Zn2+}) was measured via an Evans method[1]. The EIS of Zn||Zn symmetrical battery was collected before and after the chronoamperometry test, and calculated according to the following equation:

$$t_{z^2{}_n^+} = \frac{I_s(\Delta V - I_0 R_0)}{Io(\Delta V - I_S R_s)}$$

Where ΔV is the applied voltage polarization (25 mV). I_0 and R_0 are the initial current and resistance before polarization test. I*s* and R*s* are the steady current and resistance after the polarization.

Material characterization

Field emission scanning electron microscope (FESEM, SEM 500, China) were used for morphology analysis of the samples. X-ray diffraction (XRD) patterns were recorded on an X-ray diffractometer (Rigaku SmartLab, Cu Kα, λ=1.5418 Å) with an operating voltage of 45 kV, a current of 200 mA, and a step of 50/min. Fourier-transformed infrared spectra (FT-IR) tests were performed on Bruker Tensor-II (Germany). The morphology changes during Zn deposition and exfoliation were observed by optical microscope (YM520R, Suzhou Yueshi, China). The ionic conductivity ere measured by conductivity meter (DDSJ-308F, Lei ci, China). Proton (^{1}H NMR) nuclear magnetic resonance spectra were acquired on a JNM-ECZL400S NMR spectrometer. Raman spectra were characterized using an excitation of 532 nm at room temperature on a micro-Raman spectrometer (inVia, England).

Calculation method

Density Functional Theory (DFT) calculations were implemented using the DMol3 package in Materials Studio[2] with the Perdew−Burke−Ernzerhof (PBE)[3] exchange−correction functional within the Generalized Gradient Approximation (GGA)[4]. The Kohn–Sham wave functions were expanded in the double numerical polarization (DNP) basis on polarized atomic orbitals. Structural optimizations were performed up to the Hellmann−Feynman force on all ion of 0.005 Ha $Å^{-1}$, the total energy of 2×10^{-5} eV, and maximum atomic displacement of 0.005 Å. The self-consistent field

(SCF) procedure utilized an energy convergence threshold of 1.0×10^{-5} eV to ensure electronic structure accuracy. The binding energy was calculated through the following expression:

$$\Delta E = E_{abs\,/\,sub} - E_{abs} - E_{sub}$$

Where $E_{abs/sub}$ were the total energy of absorbate-substrate, E_{abs} and E_{sub} are the energies of the absorbate and substrate, respectively.

Molecular dynamics (MD) simulations were performed employing the Forcite module in the Material Studio. A3.6×3.6×3.6nm³ cubic simulation unit with three-dimensional periodic boundary conditions was constructed, containing 1110 H_2O molecules, 40 $ZnSO_4$ (2 M $ZnSO_4$), and 10 HACC molecules based on the stoichiometric ratio. Before applying the electric field, Forcite tool was used to systematically optimize the structural geometry of all components to ensure a stable initial configuration. The interatomic interactions were calculated using the COMPASSII force field with the following parameters: van der Waals forces were treated through the Ewald summation method (accuracy threshold: 10^{-3} kcal/mol) combined with an atom-based cubic spline truncation scheme (cutoff distance: 12.5 Å). Following structural optimization, the system underwent NVE ensemble MD simulations at 300 K, implemented with a time step of 1.0 fs for 500 ps of total simulation time[5]. The amorphous cell construction protocol included dynamic relaxation procedures to ensure proper system equilibration. Radial distribution function (RDF) analysis was subsequently conducted using Materials Studio's analytical tool, calculated through the following formulation[6]:

$$g(r) = \frac{v}{N_S N_C} \sum_{i=1}^{N_c} \frac{N_{is}(r)}{4\pi r^2 \Delta v}$$

Where N_C is the number of central atoms being surrounded, N_S is the number of the surrounding atoms of a central atom. N_{is} represents the number of the surrounding atoms in the range of r to r+△r for the i^{th} central atom. v is the volume of the system. The coordination number is calculated by integrating the RDF function g (r).

Meanwhile, we also calculated the mean square displacements (MSD) of SO_4^{2-} and Zn^{2+} in BE or HACC-BE according to the following equation[7]:

$$MSD = \langle |r(t) - r(0)|^2 \rangle = \frac{1}{N} \Sigma_{i=1}^{N} |r_i(t) - \gamma_i(0)|^2$$

Where *r*(t) is the coordinate of the particle at time t and N is the total number of calculated particles. By using another expression of MSD, we can calculate the corresponding diffusion coefficients by the following equation[8]:

$$\mathrm{MSD} = 2n_d \mathrm{D}\, t$$

Where n_d is the dimensionality of the system, i.e., in this system n_d i = 3.

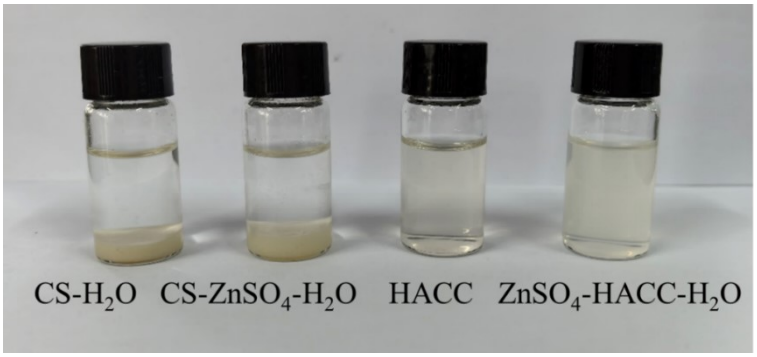

Fig. S1. Optical photographs of CS or HACC in H_2O or $ZnSO_4$ solutions.

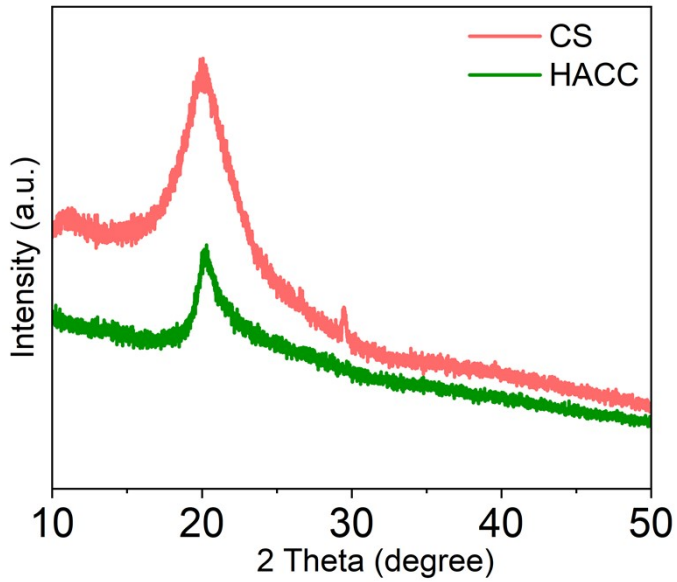

Fig. S2. XRD patterns of CS and HACC.

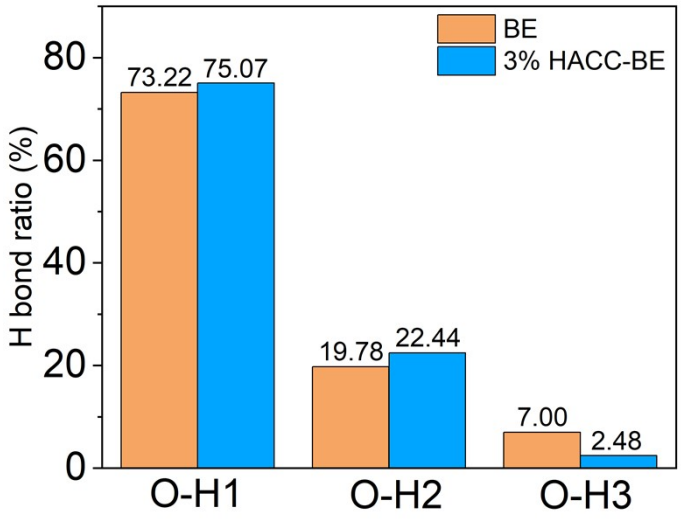

Fig. S3. Summary of hydrogen bond in BE or HACC-BE.

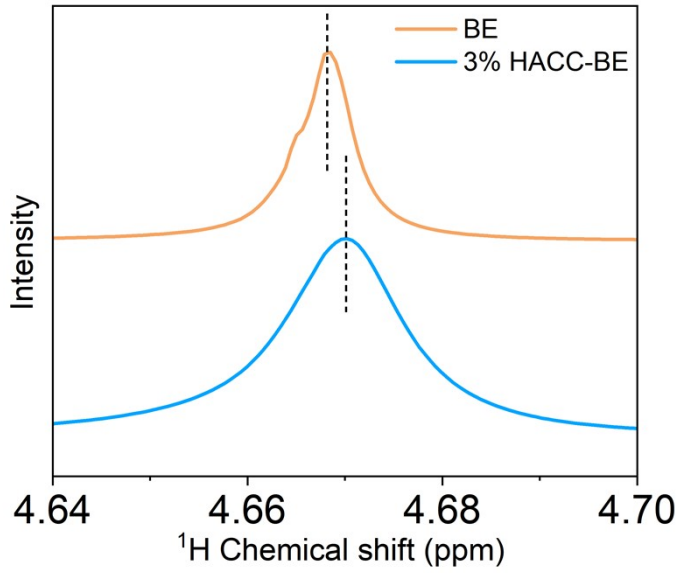

Fig. S4. ^{1}H NMR of BE and 3% HACC-BE.

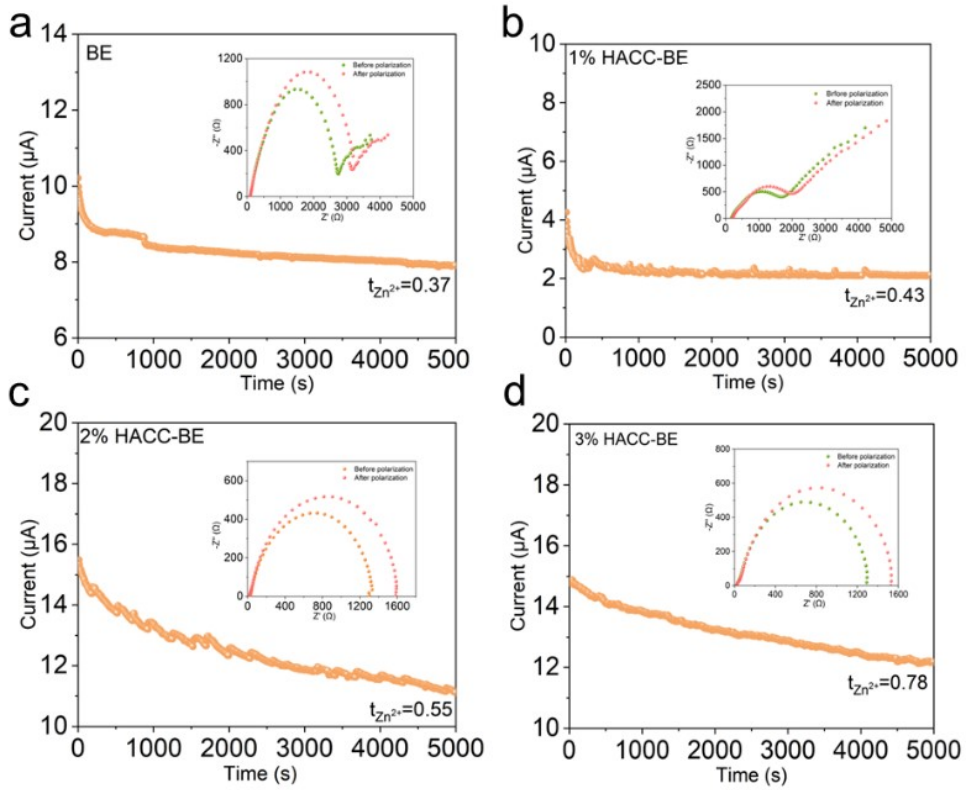

Fig. S5. Electrochemical impedance spectra before and after linear polarization. (a) BE, (b-d) HACC-BE with different content of HACC.

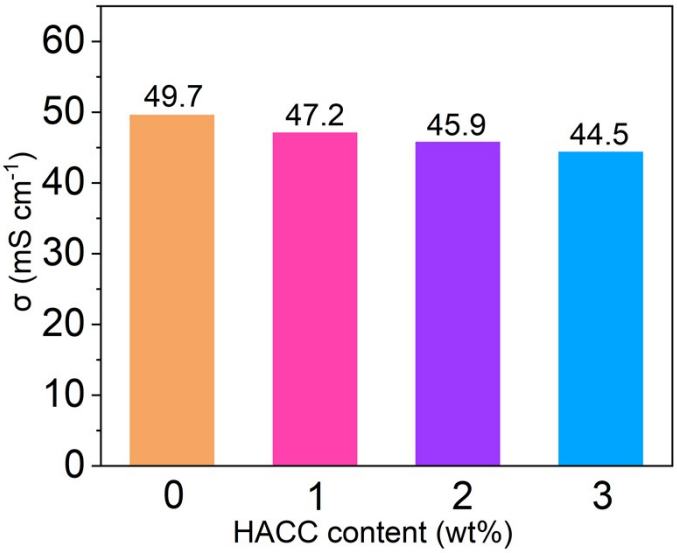

Fig. S6. Ion conductivity of electrolytes with different HACC contents.

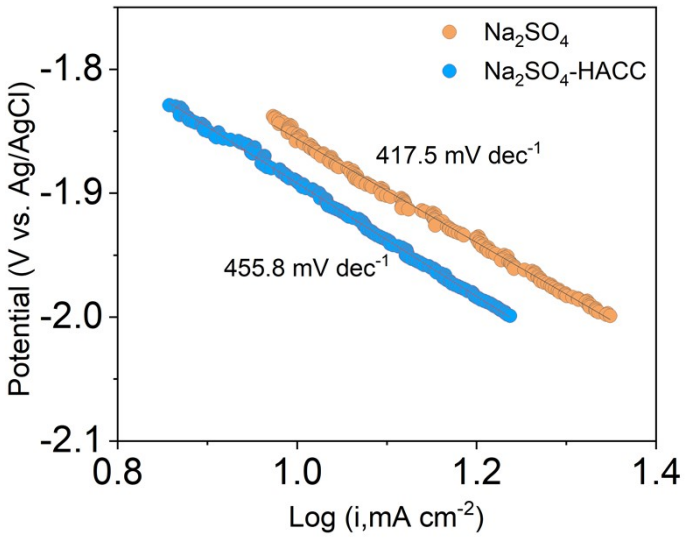

Fig. S7. Tafel slope curves of Na_2SO_4 and Na_2SO_4+HACC.

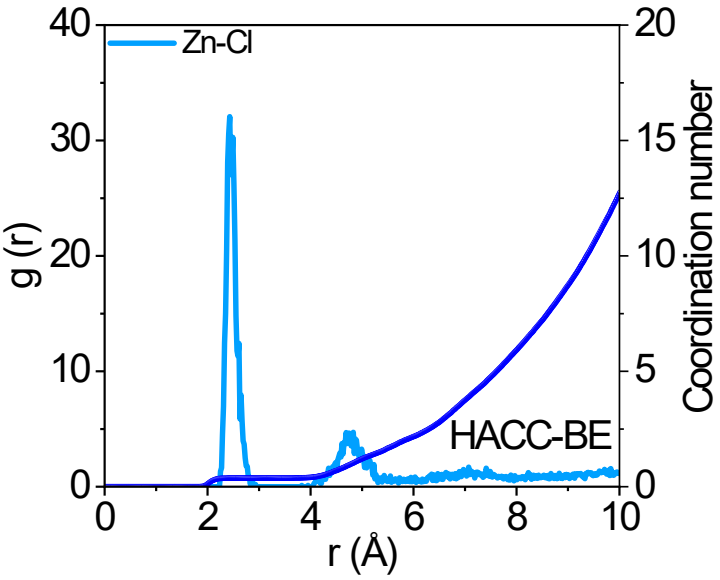

Fig. S8. The radial distribution functions and coordination number of Zn-Cl in HACC-BE.

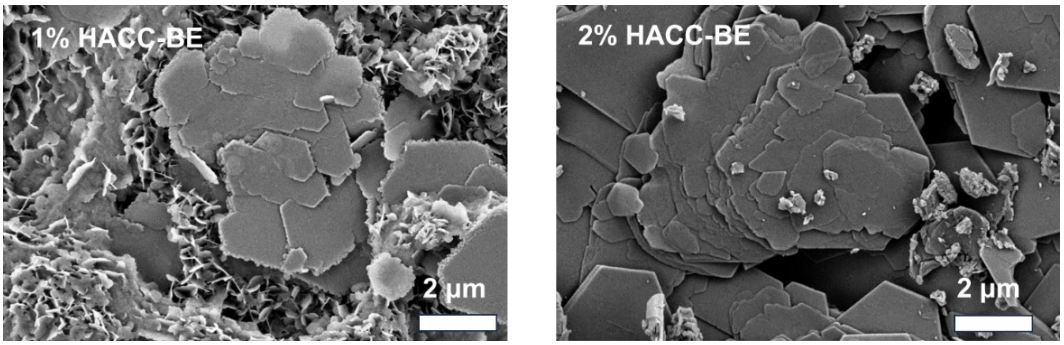

Fig. S9. SEM images of Zn anode after 100 cycles, (a) 1%HACC+BE and (b) 2%HACC+BE.

With the addition of 1 wt% HACC to the electrolyte, although minor dendritic protrusions remained, the morphology transitioned from vertical dendrites (BE) to smaller Zn platelets (Fig. S9 a), evidencing partial suppression of uncontrolled 2D diffusion. At 2 wt% HACC, horizontally oriented Zn deposits were observed (Fig.S9 b), attributed to the preferential adsorption of HACC on the Zn electrode, which redirected the deposition kinetics toward lateral growth.

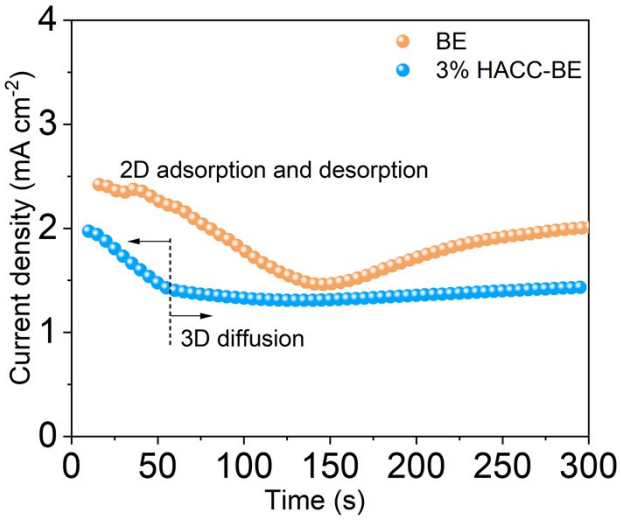

Fig. S10. Chronoamperograms of the symmetric cells using BE or HACC-BE as the electrolyte.

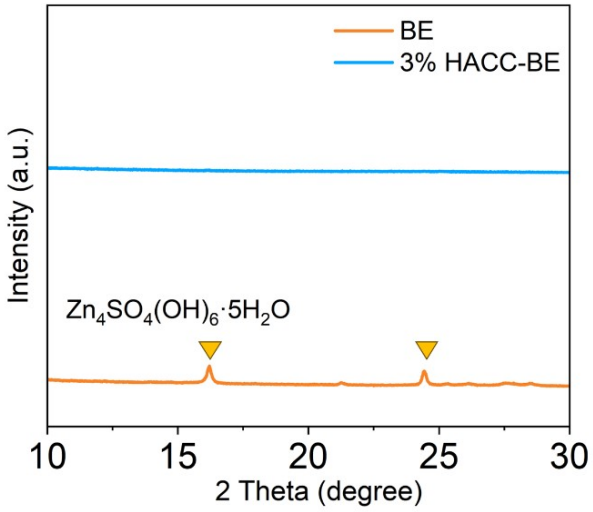

Fig. S11. XRD patterns of Zn anode after 100 cycles.

To demonstrate the formation of by-products, XRD testing was conducted on the Zn electrode after 100 cycles. The Zn electrode cycled in BE shows a distinct peak at 2θ=16° and 2θ=24°, corresponding to the by-product zinc hydroxysulfate hydrate ($Zn_4SO4(OH)_6 \cdot 5H_2O$,). In contrast, the electrode cycled in HACC-BE shows negligible intensity at this position, confirming the inhibitory effect of the HACC additive on by-product formation.

a

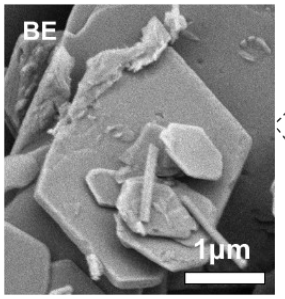

Element	Normalized mass [%]	Atom [%]
Zn	74.16	42.31
O	17.96	41.87
S	4.46	5.19
C	3.42	10.64
N	0.00	0.00
	100.00	100.00

b

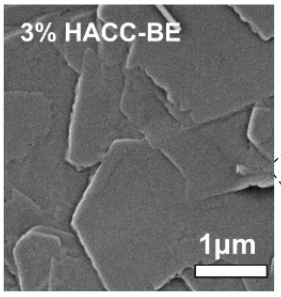

Element	Normalized mass [%]	Atom [%]
Zn	55.20	23.42
O	30.50	52.88
S	6.40	5.54
C	7.65	17.66
N	0.25	0.50
	100.00	100.00

Fig. S12. EDS of Zn anode after 100 cycles.

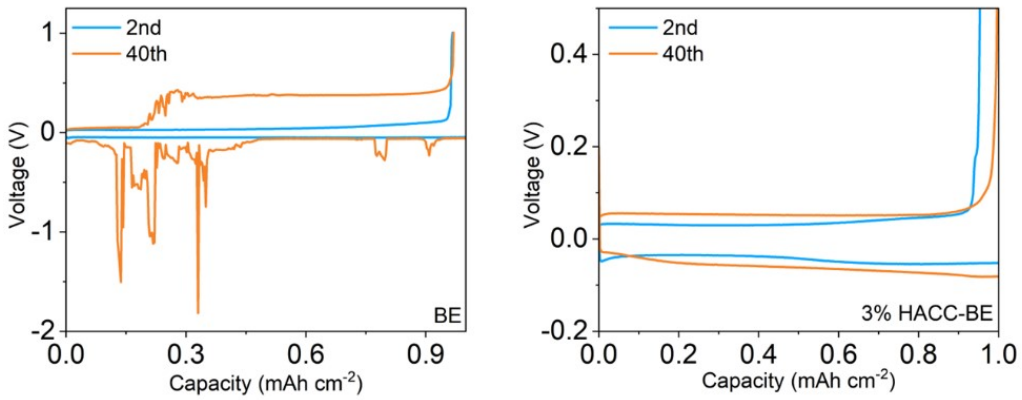

Fig. S13. Voltage profiles of Zn||Cu after different cycles at 1 mA cm^{-2} for 1mAh cm^{-2}, (a)BE and (b)3% HACC-BE.

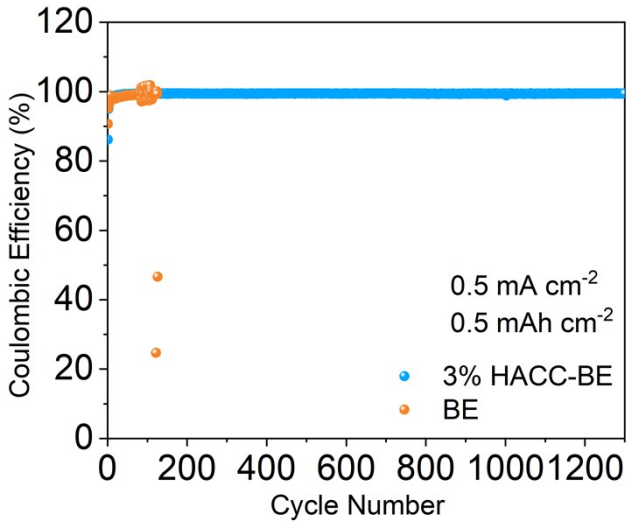

Fig. S14. Cycling performance of Zn ||Cu at 0.5 mA cm^{-2} for 0.5 mAh cm^{-2}.

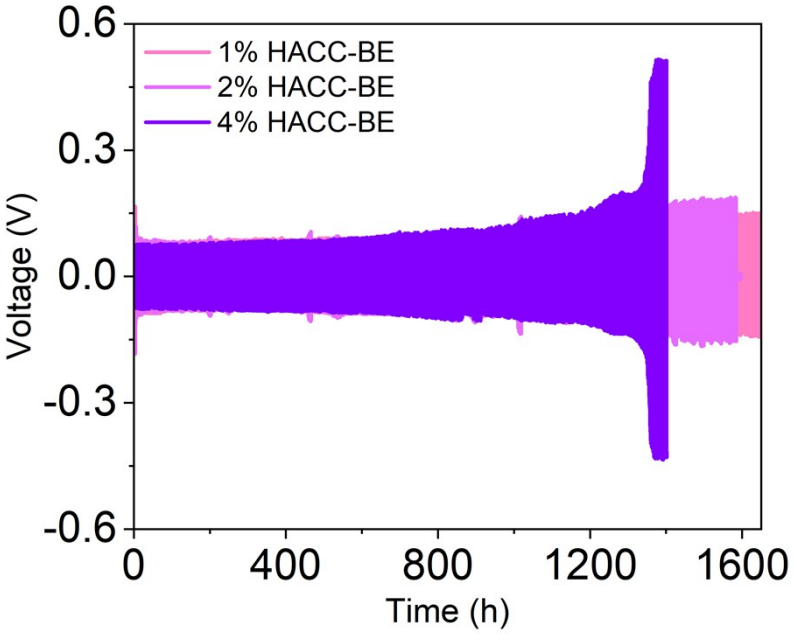

Fig. S15. Cycling performance of Zn||Zn cells with different concentrations of HACC.

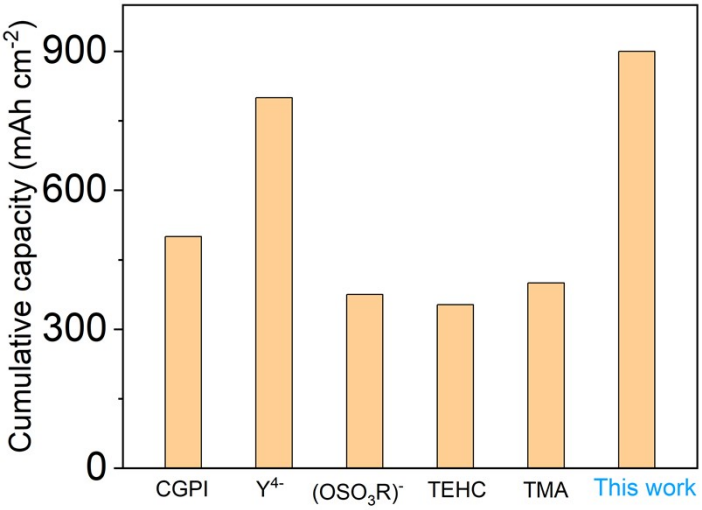

Fig. S16. Comparison of the cycling performances of Zn||Zn cells with the reported data.

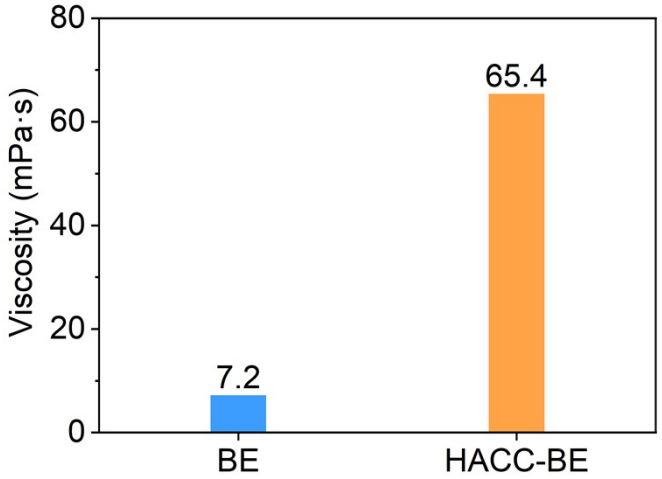

Fig.S17. Viscosity of BE and HACC-BE electrolyte.

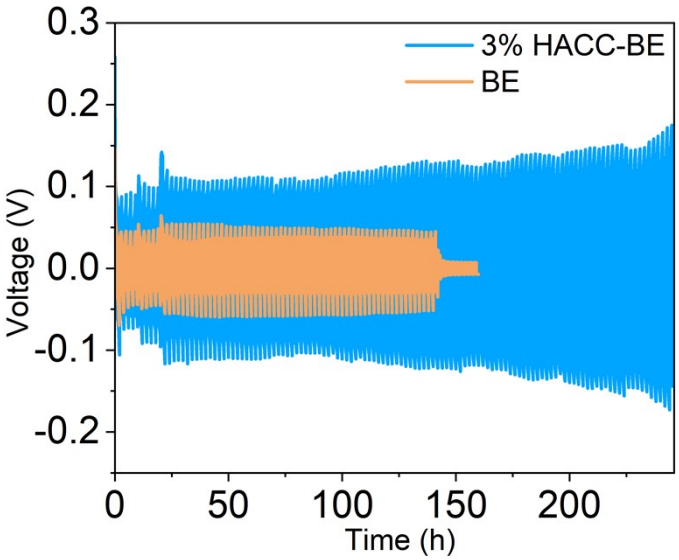

Fig. S18. Cycling performance of Zn||Zn with different electrolyte at 5 mA cm^{-2} and 5 mAh cm^{-2}.

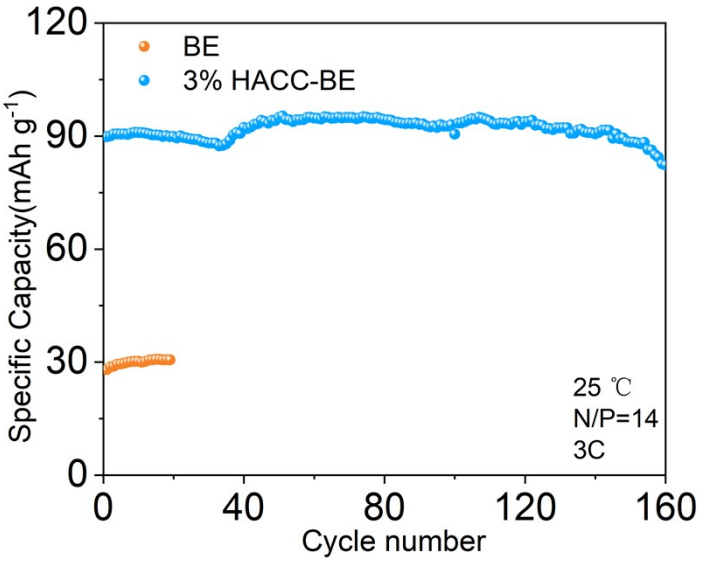

Fig. S19. Cycling performance of Zn||LMO at 3 C using different electrolytes.

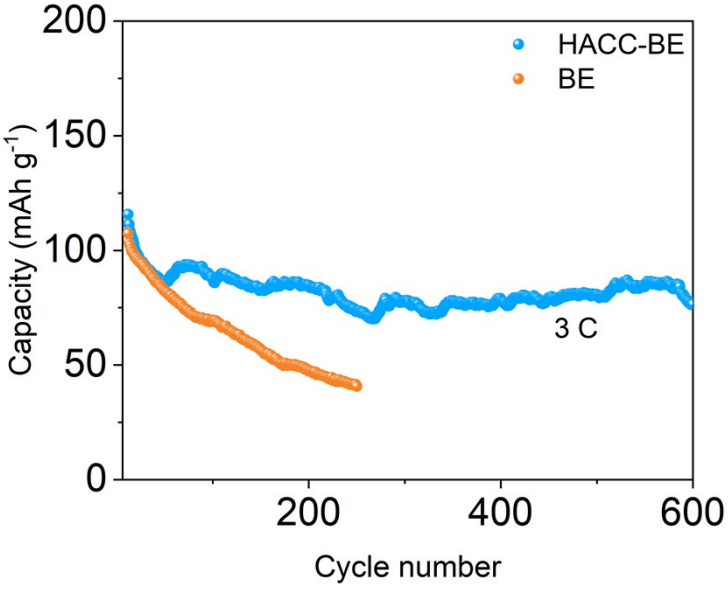

Fig. S20 Cycling performance of Zn||MnO_2 at 3 C using different electrolytes.

Table S1. Cycling performance comparison of Zn batteries with different charge additives

Electrolyte additive	Charge	Current density (mA cm^{-2})	Capacity (mAh cm^{-2})	Cumulative capacity (mAh cm^{-2})	Life time (h)	Ref.
CGPI	zwitterion	0.5	0.5	500	2000	[9]
Y^{4-}	anion	1	1	800	1600	[10]
$(OSO_3R)^-$	anion	1	0.5	375	750	[11]
TEHC	cation	1	0.5	335	670	[12]
TMA	cation	1	1	400	800	[13]
HACC	**cation**	**1**	**1**	**900**	**1800**	**This work**

References

1. Z. Cao, P. Zhuang, X. Zhang, M. Ye, J. Shen and P. M. Ajayan, Adv. Energy Mater., 2020, **10**, 2001599.

2. B. Delley, J. Chem. Phys., 2000, **113**, 7756.

3. Perdew, Burke, Wang, Phys. B Condens. Matter, 1996, **54**, 16533.

4. K. Burke, M. Ernzerhof, Phys. Rev. Lett., 1996, **77**, 3868.

5. S. Qi, H. Wang, J. He, J. Liu, C. Cui, M. Wu, F. Li, Y. Feng, J. Ma, Sci. Bull., 2021, **66**, 685.

6. W. Humphrey, A. Dalke, K. Schulten, J. Mol. Graph., 1996, **14**, 33

7. A. Muralidharan, M. I. Chaudhari, L. R. Pratt, S. B. Rempe, Sci. Rep., 2018, **8**, 1073.

8. A. R. Allouche, J. Comput. Chem., 2011, **32**, 174-182.

9. S. Deng, Y. Sun, Z. Yang, M. Wu, H. Tong, X. Nie, Y. Su, J. Li and G. Chai, Adv. Funct. Mater, 2024, **34**, 2408546.

10. S. Di, L. Miao, Y. Wang, G. Ma, Y. Wang, W. Yuan, K. Qiu, X. Nie and N. Zhang, J. Power Sources, 2022, **535**, 231452.

11. G. Guo, C. Ji, H. Mi, C. Yang, M. Li, C. Sun and L. Sun, Adv. Funct. Mater, 2023, **34**, 2308405.

12. L. Qian, W. Yao, R. Yao, Y. Sui, H. Zhu, F. Wang, J. Zhao, C. Zhi and C. Yang, Adv. Funct. Mater, 2021, **31**, 2105736.

13.L. Zheng, H. Li, M. Gao, K. Huang, J. Wang, L. Su, L. Li, H. Lin, X. Gao, Z. Liu and H. Zhang, Adv. Sci, 2024, **11**, e2407102.